Plasmon Thermal Conductance and Thermal Conductivity of Metallic Nanofilms

Jose Ordonez-Miranda, Yuriy A. Kosevich, Bong Jae Lee, Masahiro Nomura, and Sebastian Volz

Phys. Rev. Applied **19**, 044046 — Published 17 April 2023

DOI: 10.1103/PhysRevApplied.19.044046

Plasmon Thermal Conductance and Thermal Conductivity of Metallic Nanofilms

Jose Ordonez-Miranda,[1,2,*] Yury A. Kosevich,[3,2] Bong Jae Lee,[4,5] Masahiro Nomura,[2,1] and Sebastian Volz[1,2]

[1] *LIMMS, CNRS-IIS UMI 2820, The University of Tokyo, Tokyo 153-8505, Japan*
[2] *Institute of Industrial Science, The University of Tokyo, Tokyo 153-8505, Japan*
[3] *N. N. Semenov Federal Research Center for Chemical Physics of Russian Academy of Sciences, 4 Kosygin Street, Moscow 119991, Russian Federation*
[4] *Department of Mechanical Engineering,Korea Advanced Institute of Science and Technology, Daejeon 34141, South Korea*
[5] *Center for Extreme Thermal Physics and Manufacturing, Korea Advanced Institute of Science and Technology, Daejeon 34141, South Korea*

(Dated: March 17, 2023)

The thermal conductance and thermal conductivity of surface plasmon-polaritons propagating along a metallic nanofilm deposited on a substrate are quantified and analyzed, as functions of the film thickness, length, and temperature. This is done by analytically solving the dispersion relation of plasmons for their wave vectors and propagation length. It is shown that the plasmon energy transport along the film interfaces is driven by two modes characterized by symmetric and antisymmetric spatial distributions of the magnetic field. For a gold nanofilm deposited on a silicon substrate, both modes have comparable contributions of the plasmon thermal conductance, which takes higher values for hotter and/or longer nanofilms, and saturates for films thicker than 50 nm. This saturation arises from the decoupling of the plasmon modes, whose transition to a coupled state for thinner films, maximizes the plasmon thermal conductivity. For a 1-cm-long gold nanofilm at 300 K, the maximum thermal conductivity appears for a thickness of 10 nm and takes the value of 15 $\mathrm{Wm^{-1}K^{-1}}$, which is about 25% of its electron counterpart. As a result of the huge propagation distance (> 1 cm) of plasmons, this plasmon thermal conductivity significantly increases with the film length and temperature, and it could therefore be useful to improve the heat dissipation along metallic nanofilms.

I. INTRODUCTION

Heat dissipation from nanomaterials is one of the most important issues in the development of modern devices due to the usual reduction of their thermal performance as their dimensions scale down to a few tens to hundreds nanometers. In nanofilms, this reduction gets stronger for thinner films, and is generated by the decrease of their thermal conductivity that results from the increasing boundary scattering of phonons or electrons propagating inside their volumes mainly. However, as the surface-to-volume ratio ($\propto 1/\text{thickness}$) increases as the film thickness decreases, the predominant surface effects in nanofilms indicate that they could support the heat conduction not only inside their volumes but also along their interfaces. This interfacial heat transport can be driven by surface electromagnetic waves, such as the surface phonon-polaritons (SPhPs) and surface plasmon-polaritons (SPPs) that appears in polar and metallic nanofilms, respectively [1–7]. The in-plane propagation and cross-plane evanescent nature of these surface waves enable them to propagate distances (> 1 mm) much greater than the typical mean free path of phonons and electrons [8–11], at speeds close to the speed of light in vacuum [1, 2, 12, 13]. The fast and long-range surface waves can thus be powerful energy carriers capable of enhancing the in-plane heat conduction in nanofilms.

The SPhPs are generated by the coupling of infrared photons with optical phonons at the interface of polar materials [7, 14]. Previous theoretical [1, 2, 15] and experimental [16–18] works reported that the SPhP contribution to the in-plane thermal conductivity of suspended polar nanofilms can actually be comparable to or higher than its phonon counterpart. These experimental works showed that thinner [16], hotter[17], or longer[18] nanofilms exhibit a higher SPhP thermal conductivity, as predicted by theory [1, 2, 15]. This thermal performance enhancement arises from the evanescent coupling of the SPhPs propagating along the two nanofilm interfaces and their ability to propagate distances much longer than the typical lateral dimensions (~ 1 mm) of the nanofilms [2]. The SPhP coupling shows up not only in single nanofilms, but also in micro-sized structures made up of a thick silicon layer sandwiched by polar nanofilms [19]. As a result of the strong coupling of SPhPs propagating along its two SiO_2 nanofilms, this $SiO_2/Si/SiO_2$ structure can efficiently enhance the in-plane SPhP heat transport to values ten times higher than the corresponding one of a single SiO_2 nanofilm [20]. The suspended nanofilms and microscale sandwiches are symmetrical structures that support the long-range propagation of SPhPs in a broad range of frequencies [1, 2]. By contrast, for supported structures, such as a nanofilm deposited on a substrate, the propagation distance and frequency spectrum of SPhPs are significantly reduced due to the mismatch of the emissivities of its surrounding media and the existence of the SPhP resonance of polar materials [Re(permittivity) < 0] in a limited frequency interval [2]. These two reductions significantly suppress the SPhP contribution to the thermal conduc-

* jose.ordonez@cnrs.fr

tivity of supported polar nanofilms, even though they provide better conditions than suspended ones for practical use. SPhPs therefore open a heat transport channel in suspended nanofilms and symmetric structures mainly.

By analogy with polar dielectrics supporting the propagation of SPhPs, metals support the existence of SPPs, which results from the hybridization of photons and free electrons propagating near the metal interfaces [21–23]. The abundance of these free electrons in metals leads to a high plasma frequency ω_p determining the upper limit $(\omega_p/\sqrt{2})$ of the frequency spectrum supporting the propagation of SPPs [7, 23]. In contrast to polar dielectrics, the high ω_p of metals (i.e. $\omega_p/2\pi = 2196.34$ THz for gold [24, 25]) and the (relatively large) negative values of the real part of their permittivity for frequencies smaller than ω_p, enable the existence and propagation of SPPs in a very broad range of frequencies [3, 7, 26, 27]. Thermally excited SPPs are thus wide spectrum energy carriers and their cross-plane propagation was applied to enhance and tailor the near-field thermal radiation [28–30]. The impact of SPPs in heat conduction, on the other hand, is less explored [30–32]. Special attention has been dedicated to the temperature profile of plasmonic nanoparticles excited with an optical heating at a given frequency [33–35]. This single-frequency excitation generates SPPs of a unique frequency and with many observable thermal effects, however, it does not enable to fully take advantage on the broad frequency range of SPPs. The broad spectrum excitation and propagation of SPPs can be achieved with thermal sources and could significantly enhance the heat transport in metallic nanofilms, as they support the SPP propagation over distances of some centimeters [4, 36]. As metallic nanofilms with these lateral dimensions can nowadays be fabricated by depositing them on a substrate, they provide a suitable medium to capitalize on the full propagation potential of SPPs. However, despite of their close analogy with SPhPs, the contribution of SPPs to the thermal conductivity of metallic films is not explored yet.

In this work, we theoretically determine the SPP contribution to the thermal conductance and thermal conductivity of a metallic nanofilm, as functions of its thickness, length, and temperature. This is done by analytically solving the dispersion relation of SPPs for their wave vectors and propagation length. The existence of two SPP modes with propagation parameters strongly determined by the permittivity of the nanofilm surrounding media is found. For a gold nanofilm deposited on a silicon substrate, both SPP modes have comparable contributions to the SPP heat conductance, which takes higher values for hotter and/or longer nanofilms, and saturates for thicknesses greater than 50 nm.

II. THEORETICAL MODEL

Let us consider a metallic film supporting the propagation of SPPs along its interfaces with its substrate and superstate, as shown in Fig. 1. These top and bottom materials have relative permittivities ε_1 and ε_3, respectively; and they are separated by the film of relative permittivity ε_2 and thickness d. Considering that the surface $x = 0$ of the metallic film is uniformly heated up with a thermal bath or laser beam, its free electrons oscillate and emit an electromagnetic field. These oscillations induce the excitation of neighboring electrons, which keeps the field propagation along the film interfaces mainly. This thermally excited field represents a SPP able to propagate in a broad range of frequency, as reported in the literature [32, 37]. Under this condition, the heat propagates along the x axis mostly via the combined dynamics of electrons and SPPs. Given that SPPs, as SPhPs, are bosons [7], the Boltzmann transport equation establishes that the SPP contribution G to the in-plane thermal conductance of the nanofilm is given by [5]

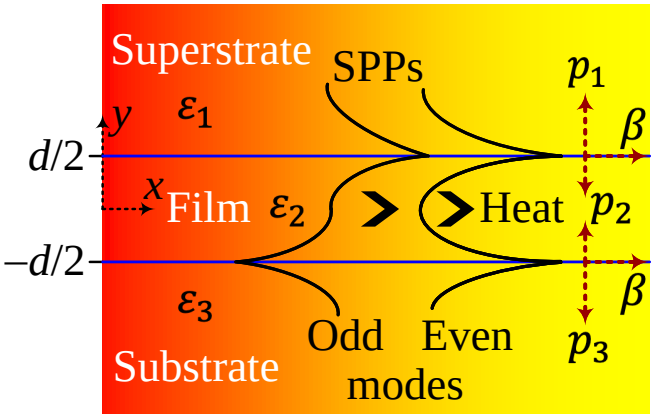

FIG. 1: Scheme of a metallic film supporting the propagation of SPPs along its interfaces with the substrate and superstrate of relative permittivities ε_1 and ε_3, respectively. The film has a relative permittivity ε_2 and thickness d. The SPPs and their heat flux propagate from the red zone (high temperature) to the yellow one (low temperature).

$$\frac{G}{a} = \frac{1}{2\pi^2}\int \hbar\omega \mathrm{Re}(\beta)\tau(\omega)\frac{\partial f}{\partial T}d\omega, \tag{1}$$

where a is the film width (dimension perpendicular to the xy plane), $\hbar$ is the Planck's constant divided by 2π, $\mathrm{Re}(\beta)$ is the real part of the in-plane SPP wave vector β, $f = [\exp(\hbar\omega/k_BT) - 1]^{-1}$ is the Bose-Einstein distribution function, T is the average temperature, k_B is the Boltzmann constant, ω is the spectral frequency, and τ is the transmission probability defined by[5]

$$\tau = \frac{\pi}{2\mu}\left(1 - \frac{4\psi(0)}{\pi\mu}\right), \tag{2}$$

where $\mu = l/\Lambda$, $\Lambda = [2\mathrm{Im}(\beta)]^{-1}$ is the in-plane SPP propagation length, and $\psi(\xi) = E_5(\xi) - E_5(\mu - \xi)$, with

$E_n(x) = \int_0^{\pi/2} \cos^{n-2}(\theta) e^{-x/\cos(\theta)} d\theta$. The transmission probability τ represents the probability that the SPPs transmit from $x = 0$ to $x = l$ along the film interfaces and its definition in Eq. (2) was derived by comparing Eq. (1) with the well-known Landauer formula for the thermal conductance of a thin film. Equation (2) thus establishes that the transmission of SPPs along the film length l is determined by μ. In the diffusive regime ($\mu = l/\Lambda \gg 1$), the ratio $\psi(0)/\mu \to 0$ and $\tau \approx 0$, while in the ballistic limit ($\mu \ll 1$), $1-4\psi(0)/\pi\mu \to 2\mu/\pi$ and $\tau \approx 1$. The SPP heat transport is hence enhanced along a film with a lateral dimension smaller than the SPP propagation length ($l \ll \Lambda$), as indicated by Eq. (1). Equation (1) was derived by considering that the temperature difference between the hot ($x = 0$) and cold ($x = l$) sides of the film is much smaller than their average temperature T [5]. For a temperature difference up to a few tens of degrees, this condition is well satisfied for temperatures comparable to or above room temperature, as is the case of practical interest. The SPP thermal conductance G (W/K) represents the thermal power (W) generated by SPPs per unit of temperature (K) and is independent of the excitation source required to excite SPPs and measure its value in a particular experiment. For an arbitrary transmission probability $\tau(\omega) = \tau(l/\Lambda) = \tau(2l\mathrm{Im}(\beta))$ ($0 < \tau < 1$) and according to Eqs. (1) and (2), the SPP thermal conductance depends on the material properties through the product $= \mathrm{Re}(\beta)\tau(2l\mathrm{Im}(\beta))$ driven by the real and imaginary parts of the SPP wave vector $\beta(\omega)$, which is given by the dispersion relation of SPPs propagating along the film shown in Fig. 1. As G increases with this product, the optimal material configuration to maximize the SPP heat transport is given by a large wave vector $\mathrm{Re}(\beta)$ and a long propagation length (small $\mathrm{Im}(\beta)$). After solving the Maxwell equations under proper boundary conditions for the transverse magnetic polarization required for the existence of SPPs[1], the following dispersion relation is obtained[7, 38]

$$\frac{p_2}{\varepsilon_2}\left(\frac{p_1}{\varepsilon_1}+\frac{p_3}{\varepsilon_3}\right)+\left(\frac{p_2^2}{\varepsilon_2^2}+\frac{p_1}{\varepsilon_1}\frac{p_3}{\varepsilon_3}\right)\tanh\left(p_2 d\right)=0, \quad (3)$$

where the cross-plane wave vectors p_n are given by $p_n^2 = \beta^2 - \varepsilon_n k_0^2$, with $k_0 = \omega/c$ and c being the wave vector and speed of light in vacuum, respectively. Equation (3) was derived by matching the tangential components of the electric and magnetic fields at the film interfaces $y = \pm d/2$ and therefore it is equally valid for finite or infinitely long films. These boundary conditions are necessary and sufficient for describing the propagation of TM waves [38]. As Eq. (3) is independent of any condition at $x = 0$, the thermal excitation of SPPs at this position could be done by considering $x = 0$ as the lateral surface of the film, as shown in Fig. 1, or as a medium position of the sample. For a very thin film ($d \to 0$), Eq. (3) becomes independent of the film parameters and reduces to the well-known dispersion relation $p_1/\varepsilon_1 + p_3/\varepsilon_3 = 0$ ($\beta = \sqrt{\varepsilon_1\varepsilon_3/(\varepsilon_1+\varepsilon_3)}$) of a single interface between the substrate and superstrate. On the other hand, for a very thick film ($|p_2|\, d \gg 1$), the SPPs propagating along the two film interfaces decouple and propagate with a wave vector $\beta_n = \sqrt{\varepsilon_n\varepsilon_2/(\varepsilon_n+\varepsilon_2)}$ for $n = 1$ and 3. None of these two limiting cases thus allow to capitalize on the SPP coupling across the film to enhance its SPP heat transport. The effect of the film thickness on G is therefore expected to appear for intermediate thicknesses mainly.

As the surface confinement of SPPs in medium $n = 1, 2, 3$ is driven by $\mathrm{Re}\,(p_n)$[38], the solution of Eq. (3) for the SPP wave vectors $\beta = k_0\sqrt{\varepsilon}$ and $p_n = k_0\sqrt{\varepsilon - \varepsilon_n}$ are generally determined by ε changing between ε_1 and ε_3. This constraint on the possible solutions for ε indicates that if the permittivity amplitude of the metallic film is much greater than the corresponding ones of its surrounding media ($|\varepsilon_2| \gg |\varepsilon_1|$ and $|\varepsilon_3|$), the transverse wave vector $p_2 = k_0\sqrt{\varepsilon - \varepsilon_2} \approx k_0\sqrt{-\varepsilon_2}$ becomes independent of the film thickness and the permittivities of the surrounding media. Under this key condition, Eq. (3) takes the form

$$\frac{\sqrt{\rho-\varepsilon_{12}}}{\varepsilon_{12}}+\frac{\sqrt{\rho-\varepsilon_{32}}}{\varepsilon_{32}}+\left(\frac{\sqrt{\rho-\varepsilon_{12}}}{\varepsilon_{12}}\frac{\sqrt{\rho-\varepsilon_{32}}}{\varepsilon_{32}}-1\right)\gamma=0. \quad (4)$$

where $\rho = \varepsilon/\varepsilon_2$, $\varepsilon_{nm} = \varepsilon_n/\varepsilon_m$, $\gamma = \tan\left(\lambda\sqrt{\varepsilon_2}\right)$, and $\lambda = k_0 d$. To better understand the solutions of Eq. (4), the following limiting cases are considered:

A. Thick film limit: $d > 4\delta_2$

Taking into account the identity $\tan(x + iy) = [\tan(x) + i\tanh(y)]\,/\,[1 - i\tan(x)\tanh(y)] = i$ for $\tanh(y) = 1$, which is well satisfied for $y > 2$, Eq. (4) can be solved with $\gamma = i$ for $\lambda\mathrm{Im}(\sqrt{\epsilon_2}) > 2$. In this case, the two solutions of Eq. (4) are given by $\sqrt{\rho - \epsilon_{n2}} = i\epsilon_{n2}$, which in terms of the effective permittivity ε yields

$$\varepsilon = \varepsilon_n\left(1-\frac{\varepsilon_n}{\varepsilon_2}\right), \quad (5)$$

with $n = 1$ and 3. The first solution ($n = 1$) is related to the SPP propagation along the superstrate-film interface, while the second one ($n = 3$) drives the propagation along the film-substrate interface. As each of these two solutions depends of the permittivity of a single surrounding material, the SPP propagation along an interface is not affected by the one along the other interface. This SPP decoupling arises due to the fact that the film thickness $d = \lambda/k_0 > 2\left[k_0\mathrm{Im}(\sqrt{\epsilon_2})\right]^{-1} = 2\left[k_0\mathrm{Re}(\sqrt{-\epsilon_2})\right]^{-1} = 4\delta_2$ is greater than four times the SPP penetration depth [38] $\delta_2 = [2\mathrm{Re}\,(p_2)]^{-1}$ inside the film. In terms of the real and imaginary parts of the film permittivity $\varepsilon_2 = \varepsilon_R + i\varepsilon_I$, this later condition reads

$$\varepsilon_I^2(\omega) > \left(\frac{4}{\lambda}\right)^2\left[\varepsilon_R(\omega)+\left(\frac{2}{\lambda}\right)^2\right]. \quad (6)$$

The parabolic inequality in Eq. (6) thus determines the range of frequencies in which Eq. (5) applies. This latter equation establishes that the cross-plane wave vectors $p_n = k_0\sqrt{\varepsilon - \varepsilon_n}$ are given by

$$\frac{p_1}{k_0\varepsilon_1} = \frac{p_3}{k_0\varepsilon_3} = \frac{1}{\sqrt{-\varepsilon_2}} = \frac{\sqrt{|\varepsilon_2| - \varepsilon_R} + i\sqrt{|\varepsilon_2| + \varepsilon_R}}{\sqrt{2}\,|\varepsilon_2|}, \tag{7a}$$

$$\frac{p_2}{k_0} = \sqrt{-\varepsilon_2} = \frac{1}{\sqrt{2}}\left(\sqrt{|\varepsilon_2| - \varepsilon_R} - i\sqrt{|\varepsilon_2| + \varepsilon_R}\right). \tag{7b}$$

Taking into account that the confinement of SPPs to both film interfaces increases with $\mathrm{Re}(p_n)$ [4, 7], Eqs. (7a) and (7b) indicate that this confinement becomes stronger in metallic films with higher absorption ($\varepsilon_I \gg 1$) and/or $\varepsilon_R \ll 0$. If the substrate and superstrate are non-absorbing media ($\mathrm{Im}(\varepsilon_1) = \mathrm{Im}(\varepsilon_3) = 0$), the real and imaginary parts of the in-plane wave vector $\beta = \beta_R + i\beta_I = k_0\sqrt{\varepsilon_n}\sqrt{1 - \varepsilon_n/\varepsilon_2} \approx k_0\sqrt{\varepsilon_n}\,(1 - \varepsilon_n/2\varepsilon_2)$, for $n = 1$ and 3, are given by

$$\beta_R = k_0\sqrt{\varepsilon_n}\left(1 - \frac{\varepsilon_n\varepsilon_R}{2\,|\varepsilon_2|^2}\right), \tag{8a}$$

$$\beta_I = k_0\frac{\varepsilon_I\sqrt{\varepsilon_n}^3}{2\,|\varepsilon_2|^2}. \tag{8b}$$

Equation (8b) indicates that the SPP propagation length $\Lambda = (2\beta_I)^{-1} \propto \varepsilon_I^{-1}\varepsilon_n^{-3/2}$ increases as the film absorption decreases ($\varepsilon_I \to 0$) and it takes longer values along the film interface with the medium of lower permittivity. This distance Λ drives the spatial decay of SPPs, as established by the intensity of their electrical field $|E|^2 \propto \exp(-x/\Lambda)$ [38]. This relation and Eq. (8b) thus indicate that the SPP decay increases with ε_I, which, for gold, is pretty much independent of temperature, for temperatures lower than 600 K [25]. Therefore, the SPP decay in gold is not expected to be significantly affected by temperature (< 600 K). However, the evanescent SPP propagation along the film interfaces enhance the heat dissipation from a hot spot and therefore lowers its temperature with respect to its value in absence of SPPs. This temperature results from the simultaneous propagation of SPPs and electrons inside the metallic film and is expected to exhibit a non-linear spatial distribution, as shown in the literature for SPhPs [5]. According to Eq. (8a), the SPPs propagate the distance Λ with a wave vector $\beta_R > 0$, for frequencies satisfying the condition $|\varepsilon_2|^2 > \varepsilon_n\varepsilon_R/2$, which yields

$$\left(\varepsilon_R - \frac{\varepsilon_n}{4}\right)^2 + \varepsilon_I^2 > \left(\frac{\varepsilon_n}{4}\right)^2. \tag{9}$$

As $\varepsilon_I > 0$, the constraint in Eq. (9) establishes that in the plane (ε_R, ε_I), the SPPs propagate outside the semicircle centered at $(\varepsilon_n/4, 0)$ with a radius $\varepsilon_n/4$. Under the thick film limit ($d > 4\delta_2$), the existence and propagation of SPPs is thus determined by Eqs. (6) and (9), respectively. Both constraints are satisfied by a relatively high imaginary part ε_I falling within the highlighted area shown in Fig. 2. Note that the values of ε_I allowing the SPP propagation are only determined by the parabolic constraint in Eq. (6), for $\varepsilon_R < 0$. This latter condition is well satisfied by the permittivity of metals in a wide frequency spectrum and therefore it is expected to facilitate an abundant presence of SPPs.

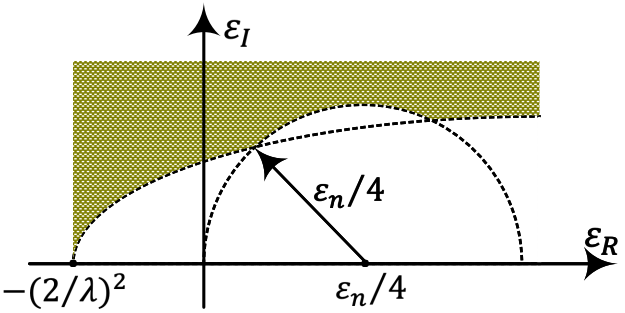

FIG. 2: Map of the region supporting the existence and propagation of SPPs along a thick film ($d > 4\delta_2$) with complex permittivity $\varepsilon_2 = \varepsilon_R + i\varepsilon_I$.

Considering that the permittivity of the metallic film is described by the Drude model, as is usually the case for a wide variety of pure metals, the frequency dependence of ε_2 is given by [7, 39]

$$\varepsilon_2(\omega) = 1 - \frac{\omega_p^2}{\omega^2 + i\Gamma\omega}, \tag{10}$$

where ω_p is the plasma frequency and Γ a damping factor driving the material energy absorption. After inserting Eq. (10) into Eqs. (7) and (8), the SPP wave vectors reduce to

$$\frac{p_1}{k_0\varepsilon_1} = \frac{p_3}{k_0\varepsilon_3} = \frac{\omega}{\sqrt{2}\omega_p}\left(\sqrt{\chi + 1} + i\sqrt{\chi - 1}\right), \tag{11a}$$

$$p_2 = \frac{\omega_p}{\sqrt{2}c}\frac{\sqrt{\chi + 1} - i\sqrt{\chi - 1}}{\chi}, \tag{11b}$$

$$\beta_R = k_0\sqrt{\varepsilon_n}\left[1 + \frac{\varepsilon_n}{2}\left(\frac{\omega}{\omega_p}\right)^2\right], \tag{11c}$$

$$\beta_I = \frac{\Gamma\sqrt{\varepsilon_n}^3}{2c}\left(\frac{\omega}{\omega_p}\right)^2. \tag{11d}$$

where $\chi = \sqrt{1 + (\Gamma/\omega)^2}$ and the practical approximation $\omega \ll \omega_p$ was used due to the relatively high plasma frequency ($\omega_p/2\pi \gtrsim 100$ THz) of usual metals[39]. In this case, for frequencies much lower than ω_p, but much higher than Γ ($\Gamma \ll \omega \ll \omega_p$), $\chi \approx 1$ and the SPP penetration depth $\delta_2 = [2\mathrm{Re}(p_2)]^{-1} \approx 0.5c/\omega_p$ inside the metal film becomes independent of frequency, as established by Eq. (11b) and is well-known in the literature [7]. For a gold film ($\omega_p/2\pi = 2196.34$ THz), for instance, this characteristic penetration depth $\delta_2 = 10.9$ nm, which indicates that the film becomes thick for the SPP propagation when its thickness $d > 4\delta_2 = 43.6$ nm. By con-

trast, the penetration depth within the surrounding media reduces to [38] $\delta_n = [2\mathrm{Re}(p_n)]^{-1} \approx c\omega_p/\varepsilon_n\omega^2$, which is inversely proportional to the square of frequency. The confinement of SPPs outside and near the two film interfaces therefore increases with the frequency ($\delta_n^{-1} \propto \omega^2$). This frequency dependence of δ_n is also exhibited by the propagation length $\Lambda = (2\beta_I)^{-1}$, which increases as the absorption parameter Γ decreases, as reported in the literature [40]. Considering that the SPPs are able to propagate a distance much longer than the film length ($\Lambda \gg l$), the transition probability in Eq. (2) becomes unity and according to Eqs. (1) and (11c), the contribution G_n of mode $n = 1$ and 3 to the SPP thermal conductance $G = G_1 + G_3$ of the metallic film is given by

$$G_n = G_0\sqrt{\varepsilon_n}\left[1 + 10\frac{z(5)}{z(3)}\varepsilon_n\left(\frac{k_bT}{\hbar\omega_p}\right)^2\right], \qquad (12)$$

where $G_0/a = 12z(3)k_B^3T^2/ch^2$ is the quantum of thermal conductance of polaritons propagating along a nanofilm[5], h is the Planck's constant, and $z(.)$ is the Riemann zeta function. Equation (12) was derived by assuming that the SPPs propagate for a wide enough frequency window to integrate the integral in Eq. (1) from 0 to ∞. The thermal conductance G_n in Eq. (12) thus represents the maximum contribution of mode n to the SPP thermal conductance. The ballistic heat transport of SPPs therefore increases with temperature and the permittivity of the surrounding media, but it takes lower values along metallic films with higher plasma frequencies, as established by Eq. (12).

B. High permittivity limit: $|\varepsilon_2| \gg |\varepsilon_1|$ and $|\varepsilon_3|$

When the amplitude of the metallic film permittivity is much greater than the ones of the surrounding media, the solution of Eq. (4) can conveniently be obtained in terms of a series expansion on $\varepsilon_{n2} = \varepsilon_n/\varepsilon_2$, regardless of the thickness d. The square roots and symmetric dependence on ε_{12} and ε_{32} of Eq. (4) indicate that its solutions for $n = 1$ and $n = 3$ accept the following expansion

$$\rho = \varepsilon_{n2} + (\alpha\varepsilon_{n2})^2\left(1 + a_1\varepsilon_{n2} + a_2\varepsilon_{n2}^2 + ...\right). \qquad (13)$$

For an approximation up to ε_{n2}^4 and $n = 1$, the combination of Eqs. (4) and (13) yields the following expressions for the parameters α, a_1 and a_2:

$$\alpha = \gamma - \frac{1+\gamma^2}{\gamma - i\sqrt{\varepsilon_{32}}}, \qquad (14a)$$

$$a_1 = \frac{\sqrt{\varepsilon_{23}}\left(1+\gamma^2\right)}{\left(\gamma - i\sqrt{\varepsilon_{32}}\right)\left(\gamma\sqrt{\varepsilon_{32}} - i\right)}, \qquad (14b)$$

$$a_2 = -\frac{\sqrt{\varepsilon_{23}}^3\left(1+\gamma^2\right)\left(\gamma\sqrt{\varepsilon_{32}}A + iB\right)}{4\left(\gamma - i\sqrt{\varepsilon_{32}}\right)^3\left(\gamma\sqrt{\varepsilon_{32}} - i\right)^2}, \qquad (14c)$$

where $A = 3 - 11\varepsilon_{32} + 4\gamma^2\left(\varepsilon_{32}^2 - 1\right)$ and $B = 4\varepsilon_{32} - \gamma^2\left(3\varepsilon_{32} + 1\right)\left(4\varepsilon_{32} - 3\right)$. These three coefficients determine all wave vectors via the effective permittivity $\varepsilon = \varepsilon_2\rho$, which, according to Eq. (13), is given by

$$\varepsilon = \varepsilon_1\left[1 + \varepsilon_{12}\alpha^2\left(1 + a_1\varepsilon_{12} + a_2\varepsilon_{12}^2\right)\right]. \qquad (15)$$

Note that ε is not only determined by the permittivities of both surrounding media but also by the film thickness d through the parameter γ. In the thick-film limit ($d > 4\delta_2$), $\gamma = i = \alpha$, $a_1 = a_2 = 0$, and Eq. (15) reduces to Eq. (5), as expected. Equation (15) thus represents the solution of the SPP dispersion relation for an arbitrary film thickness, provided that $|\varepsilon_2| \gg |\varepsilon_1|$ and $|\varepsilon_3|$. This first solution ($n = 1$) drives the propagation of SPPs along the interface with the superstrate and under the influence of the SPPs propagating along the other interface. The symmetry of Eq. (4) on ε_1 and ε_3 establishes that the second solution ($n = 3$) is related to the SPP propagation along the interface with the substrate and is given by Eqs. (14) and (15) under the exchange of the sub-indexes $1 \leftrightarrow 3$.

III. RESULTS AND DISCUSSION

The propagation and thermal properties of SPhPs propagating along a gold nanofilm deposited on a silicon substrate ($\varepsilon_3 = 11.7$) and surrounded by air ($\varepsilon_1 = 1$) are now going to be determined numerically. These two surrounding media do not absorb energy in a large frequency range [39] and therefore they favor the propagation of SPPs over long distances. On the other hand, gold is a good SPP conductor due to its high plasma frequency ($\omega_p/2\pi = 2196.34$ THz) and relatively low absorption ($\Gamma/2\pi = 15.92$ THz) [24, 25], which enable the long-range propagation of SPPs in a wide frequency range. These values of ω_p and Γ do not change significantly with temperature, for temperatures lower than 600 K and allow the Drude model to describe well the gold permittivity for frequencies lower than 2 eV = 483.6 THz [41]. This frequency windows ($\omega/2\pi < 483.6$ THz) is broad enough to cover the spectrum of the SPP thermal conductance that extends up to 50 THz mainly, as shown below.

The in-plane wave vector β_R and propagation length Λ of SPPs propagating along an gold nanofilm are respectively shown in Figs. 3(a) and 3(b), for four representative film thicknesses. The mode $n = 1$ ($n = 3$) drives the SPP propagation along the air-film (film-substrate) interface. For both modes, β_R linearly increases with frequency through values pretty much equal to the wave vector ($\sqrt{\varepsilon_n}k_0$) of light in medium n, regardless of the film thickness, for its considered values. This photon-like nature of SPPs indicates that their propagation along a film interface is nearly independent of the one along the other interface. For the mode propagating along the interface with Si, the surrounding medium with higher permittivity, small deviations from the light line are observed for the thinnest film ($d = 10$ nm) at high frequency

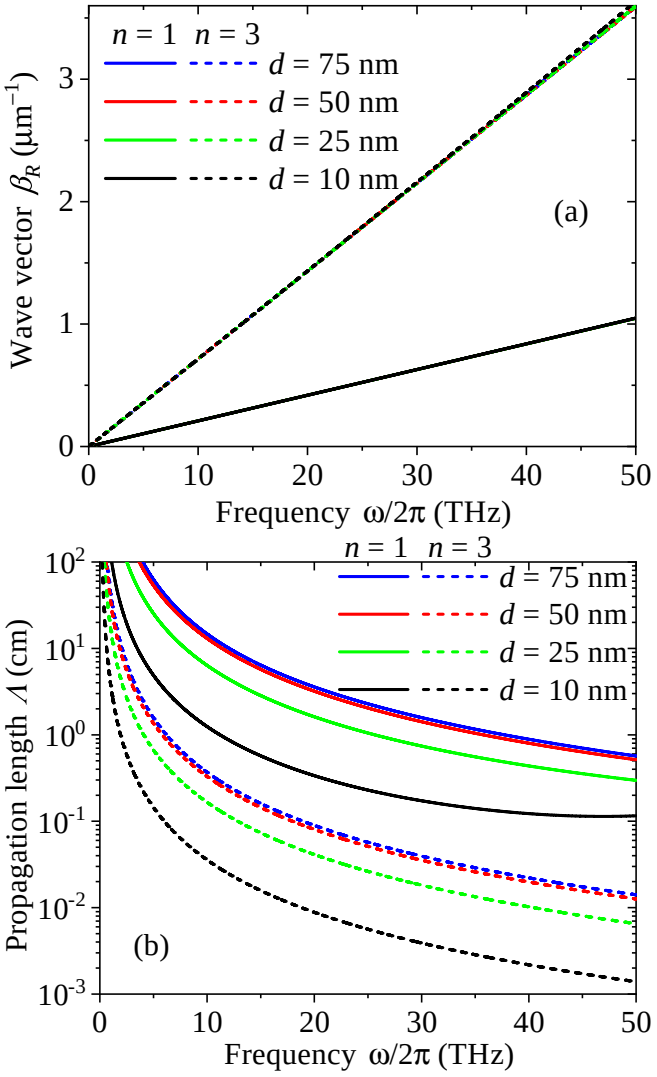

FIG. 3: Spectra of the in-plane (a) wave vector and (b) propagation length of SPPs propagating along the interfaces with air ($n = 1$) and Si ($n = 3$) of a gold nanofilm. Calculations were done for four representative film thicknesses. The continuous and dashed lines in (a) are pretty much overlapping with their corresponding black ones.

mainly, as predicted by Eq. (15). This mode ($n = 3$) exhibits the higher wave vector but the shorter propagation length with respect to mode $n = 1$, as shown in Fig. 3(b). The values of Λ increase with the film thickness and monotonically decrease as the frequency increases. In contrast to the behavior of β_R, the saturation of Λ appears for film thicker than 50 nm only. This behavior holds for both SPP modes and indicates that the coupling of SPPs propagating along the film interfaces reduces their propagation length, for films thinner than 50 nm. This destructive coupling is generated by the permittivity difference between the substrate and superstrate ($\varepsilon_3 - \varepsilon_1 = 10.7$), which increases the SPP energy loss as the film thickness decreases. The film thickness reduction thus leads to enhanced absorption resulting from the amplification of the fields inside the gold film and its broadband absorption spectrum. By contrast, for a film surrounded up and down by the same material, the SPP energy loss is lower for thinner (less absorbing) films and therefore Λ increases when the film thickness reduces, as in the case of polar nanofilms [1, 2].

Note that the SPP propagation along the gold nanofilm satisfies the condition $\mathrm{Im}(\beta) \ll \mathrm{Re}(\beta)$, which indicates that the SPP propagation length $\Lambda = [2\mathrm{Im}(\beta)]^{-1} \gg [2\mathrm{Re}(\beta)]^{-1}$ is generally greater than the in-plane wavelength $2\pi/\mathrm{Re}(\beta)$, as shown by Figs. 3(a) and 3(b). The relatively long distances ($\Lambda \sim 1$ cm) that the SPPs propagate, show their high potential to carry heat along the nanofilm interfaces, as established by Eq. (1). The reduction of the propagation length for high frequencies and thinner films is also exhibited by the SPP skin (penetration) depth into the air (δ_1) and Si (δ_3) surrounding the gold nanofilm, as shown in Figs. 4(a) and 4(c), respectively. The absorption of the SPP energy by the film hence reduces both the in-plane and cross-plane propagation distances of SPPs. SPPs with shorter (in-plane) propagation lengths are thus more confined to the film interfaces. In both surrounding media, the first SPP mode ($n = 1$) penetrates deeper than the second one ($n = 3$), such that they both go deeper into the air than into Si ($\delta_1 > \delta_3$), for a given frequency and film thickness. Note that the penetration depth of the second mode into the Si substrate is independent of the film thickness and exhibits the strongest confinement (smallest skin depth) to the film interface. The skin depth δ_2 of SPPs propagating inside the film also exhibits this thickness independence and takes values much smaller than δ_3 due to the nanofilm energy absorption, as shown in Fig. 4(b). These values of δ_2 are the same for both modes and are accurately determined by $\delta_2 = [2k_0\mathrm{Re}(\sqrt{-\varepsilon_2})]^{-1}$, which confirms the validity of the approximation ($p_2 \approx k_0\sqrt{-\varepsilon_2}$) used to derive and solve the dispersion relation in Eq. (4). As the frequency increases, δ_2 decreases and tends to $0.5c/\omega_p = 10.9$ nm, as predicted by Eq. (11b). For films thicker than 50 nm, $d > \delta_2$ for the vast majority of frequencies and therefore the SPPs propagating along both film interfaces are decoupled. This fact indicates that the SPP propagation becomes independent of the film thickness for thicknesses $d > 50$ nm, as established by Eq. (5). For thinner films, on the other hand, the intrafilm skin depth can be greater or smaller than the film thickness, within a representative frequency interval, and hence the coupling (thickness) effects show up, as shown in Figs. (3) and (4).

The contributions of the two SPP modes to the spectrum G_ω/a of the SPP thermal conductance per unit width ($G = \int G_\omega d\omega$ in Eq.(1)) of the gold nanofilm are shown in Fig. 5(a), for four representative film thicknesses. The maxima of G_ω and their frequencies of occurrence increase with the film thickness until reaching saturation for $d > 50$ nm. This saturation is related to

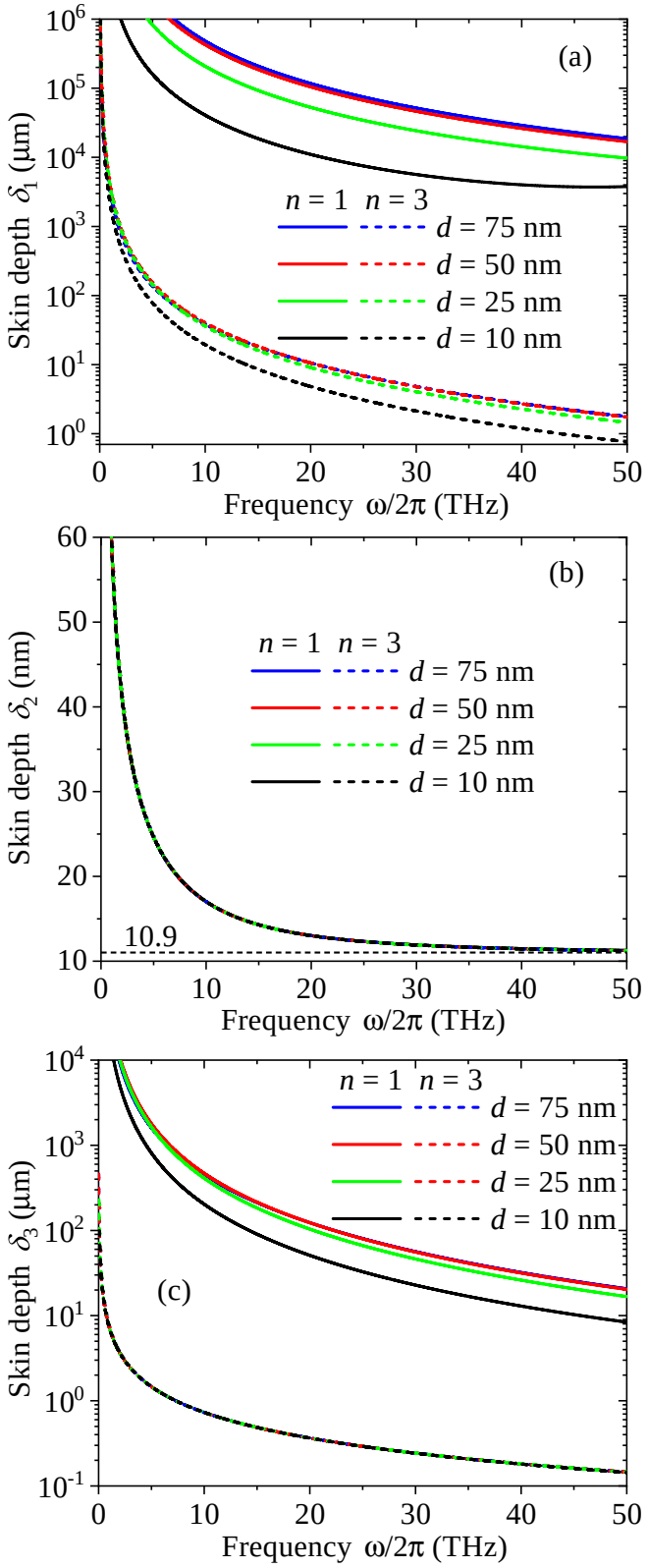

FIG. 4: Spectra of the cross-plane propagation lengths (skin depths) of SPPs propagating in (a) air (b) gold film, and (c) its Si substrate for the modes $n = 1$ and 3. The continuous and dashed lines in (b) and the dashed ones in (c) are overlapped.

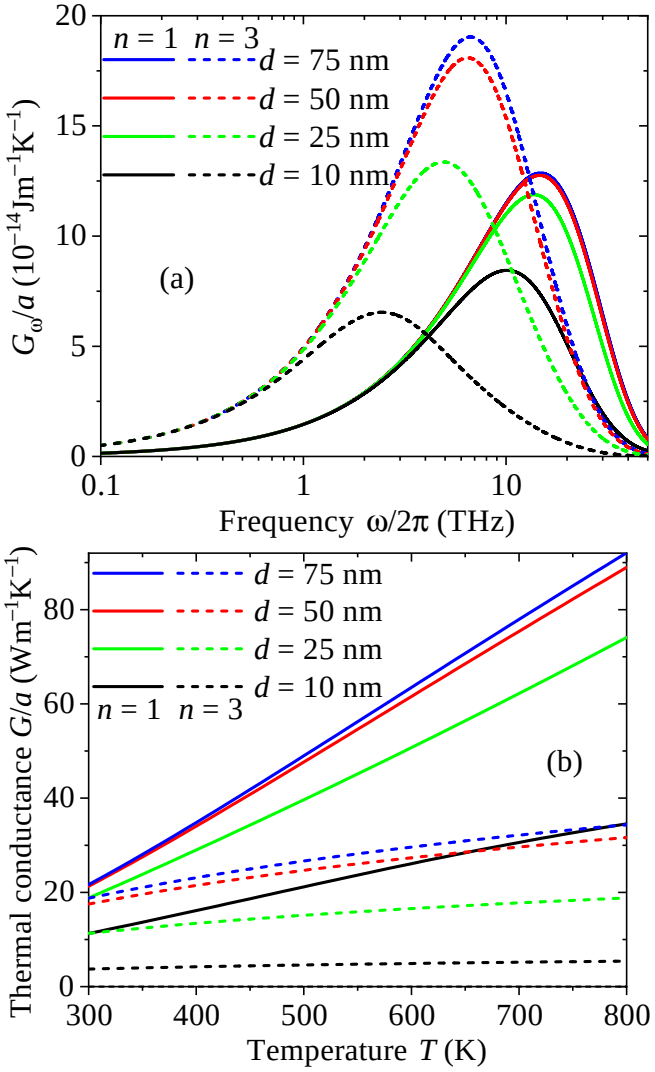

FIG. 5: (a) Spectrum of the SPP thermal conductance of a 1-cm-long gold nanofilm and its (b) integrated counterpart as a function of temperature. Calculations were done for both SPP modes, four film thicknesses, and $T = 300$ K in (a).

the one of the propagation length (see Fig. 3(b) and Eq. (1)) and arises from the decoupling ($d > \delta_2$) of the plasmon modes propagating along the two film interfaces, as shown in Fig. 4(b). These peak frequencies maximize both β_R and Λ, and therefore their vicinity provides the major contribution to the SPP thermal conductance. For frequencies higher than a given peak frequency, the sharp reduction of G_ω is driven by the exponential decrease of the Bose-Einstein distribution function (see Eq. (1)), such that its values nearly vanish for $\omega/2\pi > 50$ THz. For a given film thickness, the peak frequency of mode $n = 1$ is higher than that of mode $n = 3$, which has a higher amplitude than the former one, for $d \geq 25$ nm. This fact indicates that both modes have a significant contribution to G, as shown in Fig. 5(b). Note that the

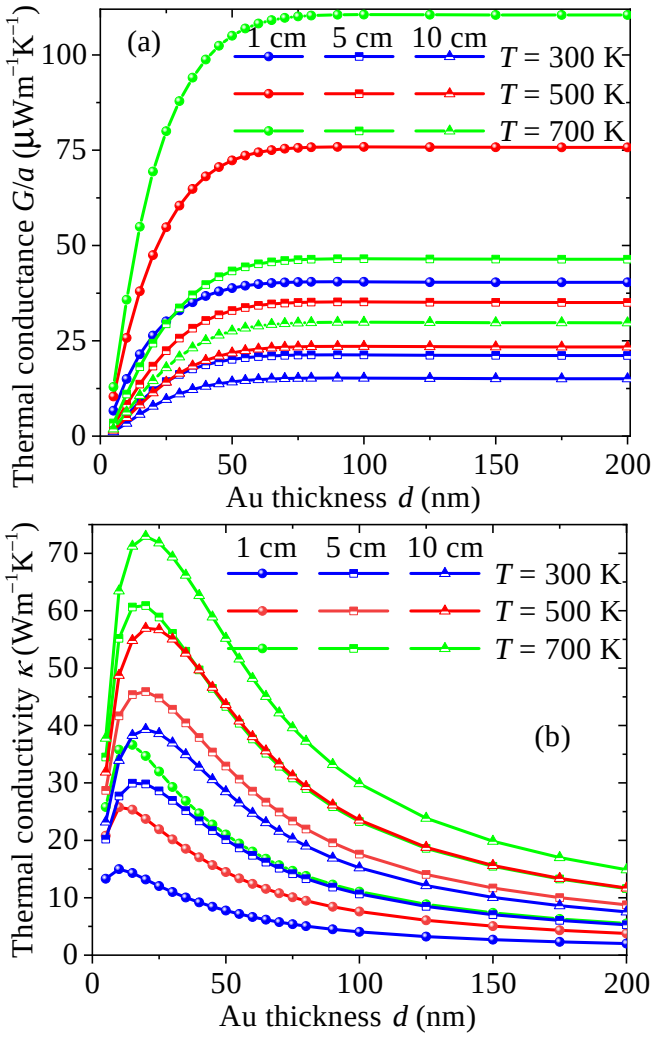

FIG. 6: (a) SPP thermal conductance per unit width and (b) thermal conductivity of a gold nanofilm as functions of its thickness. Calculations were done by summing the contributions of the two SPP modes predicted by Eq. (3), for film lengths of 1, 5, and 10 cm; and three representative temperatures.

contribution of mode $n = 1$ is generally higher than the one of mode $n = 3$, especially at high temperature. The near-linear increase of G with temperature deviates from the quadratic one predicted by Eq. (12) for the ballistic regime ($l \ll \Lambda$), because the propagation length shown in Fig. 3(b) takes smaller and greater values than the film length $l = 1$ cm considered in Fig. 5(b). This fact indicates that in the intermediate ballistic-diffusive regime, the SPP thermal conductance increases with temperature slower than in the pure ballistic one.

The sum of the contributions of both SPP modes to the SPP thermal conductance G per unit width of the gold nanofilm is shown in Fig. 6(a), as a function of its thickness d. Note that G increases with d until reaching a plateau for $d > 50$ nm, due to the uncoupling ($d > \delta_2$) of the SPP modes propagating along the film interfaces, as shown in Fig. 4(b). This maximum G value increases with the film length and temperature, as a result of the longer propagation distance in a wider frequency range, as established by the Bose-Einstein distribution function in Eq. (1). Given that our calculations are done with temperature-independent properties, the strong enhancement of G with temperature is driven by the relatively board frequency spectrum (from 0 to 50 THz mainly) supporting the flow of the SPP thermal energy, as shown in Fig. 5(a). Given that the upper bound of this thermal spectrum is much smaller than the gold plasma frequency (50 THz$\ll \omega_p/2\pi = 2196.34$ THz), the frequency spectrum of the SPP thermal conductance is not limited by ω_p, which results in the absence of the saturation of G at high temperature, for the considered temperatures in Fig. 6. For thinner films ($d < 50$ nm), on the other hand, G decreases with d as a consequence of the destructive coupling of SPPs propagating along the film interfaces. In terms of the thermal conductivity $\kappa = Gl/ad$, the coupling-uncoupling transition of G appears as a maximum due to its division by the film thickness d. This maximum appears for a film thickness increasing with temperature and film length, as shown in Fig. 6(b). For a 1-cm-long nanofilm at 300 K, a maximum thermal conductivity of 15 $\mathrm{Wm^{-1}K^{-1}}$ appears at the thickness of 10 nm. This SPP thermal conductivity is about 25% of its electron counterpart [42–44], and takes higher values for longer and/or hotter films, without increasing its thickness ($d < 25$ nm) significantly. The sizable increase of the SPP thermal conductivity with its relatively long length, while its electron counterpart keeps independent of it, indicates that the SPPs can be powerful heat carriers able to enhance the in-plane heat transport of metallic films, especially at temperatures higher than room temperature.

The SPP thermal conductivity could be measured by means of the micro time-domain thermoreflectance (μTDTR) or the steady-state thermoreflectance (SSTR) methods, which have been used to experimentally probe the polariton thermal conductivity of suspended SiN membranes [17] and supported Ti nanofilms [32], respectively. These heat-dissipation-based techniques measure the local temperature drop at a heated spot of samples. Whether the polariton heat transport is diffusive or ballistic, it enhances the heat dissipation from the heated spot and therefore lowers its temperature with respect to its value in absence of polaritons. This enhanced dissipation is thus expected to allow probing the predicted SPP thermal conductivity by fitting the measured temperature to a proper heat transport model.

IV. CONCLUSIONS

Based on the Maxwell equations of electromagnetism and the Boltzmann transport equation, the plasmon thermal conductance and thermal conductivity of a metallic

nanofilm deposited on a substrate have been quantified and analyzed, as functions of the film thickness, length, and temperature. It has been shown that the propagation of surface plasmon-polaritons along the film interfaces is driven by two modes related to the nanofilm surrounding media. For a gold nanofilm deposited on a silicon substrate, both plasmon modes have comparable contributions to the plasmon thermal conductance, which saturates for thicknesses greater than 50 nm. This saturation arises from the decoupling of the plasmon modes, whose coupling for thinner films maximizes the SPP thermal conductivity. For a 1-cm-long gold nanofilm at 300 K, the maximum thermal conductivity appears for a thickness of 10 nm and takes the value of 15 $\mathrm{Wm^{-1}K^{-1}}$, which is about half of its electron counterpart. As a result of the huge propagation distance ($>$ 1 cm) of plasmons, higher plasmon thermal conductivities are obtained for longer and/or hotter nanofilms, without significantly increasing its thickness ($<$ 25 nm). The obtained results thus show that the surface plasmon-polaritons are powerful energy carriers able to enhance the heat conduction along metallic nanofilms.

V. ACKNOWLEDGMENTS

This work was supported by the CREST Japan Science and Technology Agency, grants n° JPMJCR19Q3 and JPMJCR19I1, and the French project ANR-19-CE09-0005 "EPolariton". This work was also supported by the JSPS core-to-core program (grant n°: JPJSCCA20190006) and the Russian Academy of Sciences (Project n° FFZE-2022-0009).

[1] D.-Z. A. Chen, A. Narayanaswamy, and G. Chen, Surface phonon-polariton mediated thermal conductivity enhancement of amorphous thin films, Phys. Rev. B **72**, 155435 (2005).

[2] J. Ordonez-Miranda, L. Tranchant, T. Tokunaga, B. Kim, B. Palpant, Y. Chalopin, T. Antoni, and S. Volz, Anomalous thermal conductivity by surface phonon-polaritons of polar nano thin films due to their asymmetric surrounding media, J. Appl. Phys. **113**, 084311 (2013).

[3] Yu. A. Kosevich, Electrodynamic properties of interface between media and surface electromagnetic waves on a plane defect of a crystal, Zh. Eksp. Teor. Fiz. [JETP 69, 200 (1989)] **96**, 353 (1989).

[4] F. Yang, J. R. Sambles, and G. W. Bradberry, Long-range surface modes supported by thin films, Phys. Rev. B **44**, 5855 (1991).

[5] Y. Guo, S. Tachikawa, S. Volz, M. Nomura, and J. Ordonez-Miranda, Quantum of thermal conductance of nanofilms due to surface-phonon polaritons, Phys. Rev. B **104**, L201407 (2021).

[6] J. Ordonez-Miranda, L. Tranchant, B. Kim, Y. Chalopin, T. Antoni, and S. Volz, Quantized thermal conductance of nanowires at room temperature due to zenneck surface-phonon polaritons, Phys. Rev. Lett. **112**, 055901 (2014).

[7] V. M. Agranovich, *Surface Polaritons* (Elsevier, Amsterdam, 2012).

[8] J. Ordonez-Miranda, L. Tranchant, S. Gluchko, and S. Volz, Energy transport of surface phonon polaritons propagating along a chain of spheroidal nanoparticles, Phys. Rev. B **92**, 115409 (2015).

[9] D. Z. A. Chen and G. Chen, Measurement of silicon dioxide surface phonon-polariton propagation length by attenuated total reflection, Appl. Phys. Lett. **91**, 121906 (2007).

[10] J. Ordonez-Miranda, L. Tranchant, T. Antoni, Y. Chalopin, and S. Volz, Thermal conductivity of nano-layered systems due to surface phonon-polaritons, J. Appl. Phys. **115**, 054311 (2014).

[11] S. Gluchko, B. Palpant, S. Volz, R. Braive, and T. Antoni, Thermal excitation of broadband and long-range surface waves on sio2 submicron films, Appl. Phys. Lett. **110**, 263108 (2017).

[12] I. V. Andreev, V. M. Muravev, N. D. Semenov, and I. V. Kukushkin, Observation of acoustic plasma waves with a velocity approaching the speed of light, Phys. Rev. B **103**, 115420 (2021).

[13] Yu. A. Kosevich, A. M. Kosevich, and J. C. Granada, Magnetoplasma oscillations of a two-dimensional electron layer in a bounded system, Phys. Lett. A **1988**, 52 (1988).

[14] J. Ordonez-Miranda, L. Tranchant, K. Joulain, Y. Ezzahri, J. Drevillon, and S. Volz, Thermal energy transport in a surface phonon-polariton crystal, Phys. Rev. B **93**, 035428 (2016).

[15] J. Ordonez-Miranda, L. Tranchant, B. Kim, Y. Chalopin, T. Antoni, and S. Volz, Effects of anisotropy and size of polar nano thin films on their thermal conductivity due to surface phonon-polaritons, Appl. Phys. Express **7**, 035201 (2014).

[16] L. Tranchant, S. Hamamura, J. Ordonez-Miranda, T. Yabuki, A. Vega-Flick, F. Cervantes-Alvarez, J. J. Alvarado-Gil, S. Volz, and K. Miyazaki, Two-dimensional phonon polariton heat transport, Nano Lett. **19**, 6924–6930 (2019).

[17] Y. Wu, J. Ordonez-Miranda, S. Gluchko, R. Anufriev, D. D. S. Meneses, L. D. Campo, S. Volz, and M. Nomura, Enhanced thermal conduction by surface phonon-polaritons, Sci. Adv. **6**, eabb4461 (2020).

[18] Y. Wu, J. Ordonez-Miranda, L. Jalabert, S. Tachikawa, R. Anufriev, H. Fujita, S. Volz, and M. Nomura, Observation of heat transport mediated by the propagation distance of surface phonon-polaritons over hundreds of micrometers, Appl. Phys. Lett. **121**, 112203 (2022).

[19] S. Tachikawa, J. Ordonez-Miranda, Y. Wu, L. Jalabert, R. Anufriev, S. Volz, and M. Nomura, In-plane surface phonon-polariton thermal conduction in dielectric multilayer systems, Appl. Phys. Lett. **121**, 202202 (2022).

[20] S. Tachikawa, J. Ordonez-Miranda, Y. Wu, L. Jalabert, R. Anufriev, S. Volz, and M. Nomura, High surface phonon-polariton in-plane thermal conductance along

coupled films, Nanomaterials **10**, 1383 (2020).
[21] H. Raether, *Surface Plasmons on Smooth and Rough Surfaces and on Gratings* (Springer-Verlag, Berlin, 1988).
[22] D. Sarid and W. A. Challener, *Modern Introduction to Surface Plasmons. Theory, Mathematica Modeling and Applications* (Cambridge University Press, Cambridge, 2010).
[23] L. D. Landau, E. M. Lifshitz, and L. P. Pitaevskii, *Electrodynamics of Continuous Media* (Butterworth-Heinemann, Oxford, 1984).
[24] N. W. Ashcroft and N. D. Mermin, *Solid State Physics* (Harcout College Publishers, Forth worth, Philadelphia, 1976).
[25] A. Alabastri, S. Tuccio, A. Giugni, A. Toma, C. Liberale, G. Das, F. D. Angelis, E. D. Fabrizio, and R. P. Zaccaria, Molding of plasmonic resonances in metallic nanostructures: Dependence of the non-linear electric permittivity on system size and temperature, Materials **6**, 4879 (2013).
[26] T. Ando, A. B. Fowler, and F. Stern, Electronic properties of two-dimensional systems, Rev. Mod. Phys. **54**, 437 (1982).
[27] Y. Monarkha and K. Kono, *Two-Dimensional Coulomb Liquids and Solids* (Springer-Verlag, Berlin, 2004).
[28] V. B. Svetovoy, P. J. van Zwol, and J. Chevrier, Plasmon enhanced near-field radiative heat transfer for graphene covered dielectrics, Phys. Rev. B **85**, 155418 (2012).
[29] S. Jin, M. Lim, S. S. Lee, and B. J. Lee, Hyperbolic metamaterial-based near-field thermophotovoltaic system for hundreds of nanometer vacuum gap, Opt. Express **24**, A635 (2016).
[30] P. Ben-Abdallah, K. Joulain, J. Drevillon, and C. Le Goff, Heat transport through plasmonic interactions in closely spaced metallic nanoparticle chains, Phys. Rev. B **77**, 075417 (2008).
[31] R. Fazio, F. W. J. Hekking, and D. E. Khmelnitskii, Anomalous thermal transport in quantum wires, Phys. Rev. Lett **80**, 5611 (1998).
[32] D.-M. Kim, S. Choi, J. Cho, M. Lim, and B. J. Lee, Boosting thermal conductivity by surface plasmon polaritons propagating along a thin ti film, arXiv , 2207.09550 (2022).
[33] G. Baffou, R. Quidant, and C. Girard, Thermoplasmonics modeling: A green's function approach, Phys. Rev. B **82**, 165424 (2010).
[34] G. Baffou, R. Quidant, and F. J. Garcia de Abajo, Nanoscale control of optical heating in complex plasmonic systems, ACS Nano **4**, 709 (2010).
[35] A. Lalisse, G. Tessier, J. Plain, and G. Baffou, Plasmonic efficiencies of nanoparticles made of metal nitrides (tin, zrn) compared with gold, Scientific Reports **6**, 38647 (2016).
[36] J. J. Burke, G. I. Stegeman, and T. Tamir, Surface-polariton-like waves guided by thin, lossy metal films, Phys. Rev. B **33**, 5186 (1986).
[37] M. Lim, J. Song, S. S. Lee, and B. J. Lee, Tailoring near-field thermal radiation between metallo-dielectric multilayers using coupled surface plasmon polaritons, Nat. Commun. **9**, 4302 (2018).
[38] C. Yeh and S. F. I., *The Essence of Dielectric Waveguides* (Springer, New York, 2008).
[39] E. D. Palik, *Handbook of Optical Constants of Solids* (Academic Press, Orlando, Florida, 1985).
[40] M. S. Tomas and Z. Lenac, Thickness dependence of the surface-polariton relaxation rates in a crystal slab, Solid State Commun. **44**, 937 (1982).
[41] Y. Li, *Plasmonic Optics: Theory and Applications* (SPIE Press, Bellingham, Washington, 2017) Chap. 1.
[42] G. Chen and P. Hui, Thermal conductivities of evaporated gold films on silicon and glass, Appl. Phys. Lett. **74**, 2942 (1999).
[43] J. M. Lugo and A. I. Oliva, Thermal properties of metallic films at room conditions by the heating slope, J. Thermophys. Heat Trans. **30**, 452 (2016).
[44] H. Lin, S. Xu, C. Li, H. Dong, and X. Wang, Thermal and electrical conduction in 6.4 nm thin gold films, Nanoscale **5**, 4652 (2013).